15TH IEA HEAT PUMP CONFERENCE
MAY 26–29, 2026 | HOFBURG
VIENNA 2026
DECARBONISATION THROUGH INNOVATION

Experimental study of the ejector structural parameters on the dynamic operating characteristics of heat pump dryer system

Lingeng Zou [a], Mengqi Yu [a,b], Ye Liu [a, c], Jianlin Yu* [a, c]

a. Department of Refrigeration & Cryogenic Engineering, School of Energy and Power Engineering, Xi'an Jiaotong University, Xi'an 710049, China
b. Wuxi Little Swan Electric Company, Midea Group
c. MOE Key Laboratory of Cryogenic Technology and Equipment, Xi'an Jiaotong University, Xi'an 710049, China

Abstract

A new designed solar assisted ejector enhanced heat pump dryer system (SE-HPD) with closed-loop drying chamber has been experimentally investigated. In the SE-HPD, a hot water cycle system has been designed to simulate the solar collector. This study experimentally investigated the effects of ejector structural parameters on the dynamic operational characteristics of SE-HPD. The effects of nozzle throat diameter, mixing chamber throat diameter, and nozzle exit position (NXP) on dehumidification performance, heating efficiency, and ejector performance were analyzed. Experimental results demonstrated that the system performed best when the nozzle throat diameter was 2.21 mm (adjusting the nozzle needle displacement to 1.8 mm), achieving a moisture extraction rate (MER) of 1.65 kg·h^{-1}, a specific moisture extraction rate (SMER) of 1.76 kg·(kWh)$^{-1}$, and the highest heating COP of 3.62. However, small nozzle throat diameters (<2.21 mm) resulted a sharp decline in ejector entrainment capacity, reducing refrigerant flow rate and causing a 14.8% reduction in heating capacity. Increasing the mixing chamber throat diameter to 5 mm enhanced MER and SMER to 1.60 kg·h-1 and 1.63 kg·(kWh)-1, respectively, while further increase to 6 mm occurred vortex effects that reduced entrainment performance by 12.3%. Moreover, an NXP of 5 mm achieved the highest entrainment ratio (0.52), whereas excessive NXP (>5 mm) caused primary flow jet impingement on the mixing chamber wall, reducing the entrainment ratio to 0.31. Importantly, the study revealed the synergistic matching relationship between mixing chamber throat diameter and nozzle throat diameter: larger mixing chamber required an increased optimal nozzle diameter, with a critical area ratio (AR) optimum value. These findings provide essential experimental insights for dynamically optimizing ejector configurations in heat pump drying system.

Selection and/or peer-review under the responsibility of the organizers of the 15th IEA Heat Pump Conference 2026.

Keywords: Ejector; Heat pump dryer; Dynamic operation characteristics; Entrainment ratio; Area ratio;

Nomenclature

Nomenclature			
A	Area (m^2)	T	temperature sensor
C_p	specific heat of water (kJ·kg^{-1}K^{-1})	t_d	drying time (min)
D_m	throat diameter of the mixing chamber	U	relative uncertainty
NXP	nozzle exit position	u	uncertainty
EV	electronic expansion valve	W	electricity consumption
F_R	heat removal factor	**Greek letters**	
G	solar radiation intensity (W·m^{-2})	η	efficiency
H	Humidity sensor	ρ	density (kg·m^{-3})
MC	moisture content	μ	entrainment ratio of ejector
MER	moisture extract ratio (kg·h^{-1})	**Subscripts**	
m_d	mass of drying product (kg)	a	ambient temperature
m_{pt}	mass of product at any time (kg)	b	by-pass return air
m_w	moisture loss from the product (kg)	c	compressor
OP	opening of the EV2	con	condenser
P	Pressure (kPa)	f	fan
Q	heat (W)	in	inlet
Q_{eva}	heat absorbs from the evaporator (W)	m	main return air
Q_h	heat transfer in double-pipe heat exchanger (W)	opt	optimum
$Q_{h,sim}$	simulated solar energy (W)	out	outlet

q	flow rate of water (L·min^{-1})	sc	solar collector
r_{pj}	pressure lift ratio of ejector	w	water
SMER	specific moisture extract ratio (kg·kWh^{-1})		

1. Introduction

The application of drying technology involves agriculture, industry and daily life. Its purpose is to remove the excess water in agricultural and industrial products, and the dried products are easy to process, store, and transport. The product drying usually includes many methods such as the electrical heating drying, hot air drying, infrared radiation drying and heat pump drying (HPD) [1, 2]. Compared with the conventional drying methods, the HPD shows energy-saving potential because it can convert the heat from the surroundings into the heating capacity, resulting in a higher drying performance [3]. As the development of economy, there is a lot of energy consumed in the product drying and it contributes about 12 %-15 % to the total energy consumption of industrial [4]. Therefore, several researches have been proposed to enhanced the HPD' drying performances by modifying the heat pump cycle, improving the circulating air state, selecting the alternative refrigerants and optimizing the system components.

Besides the component optimization for conventional HPD systems, solar energy has been widely used in HPD systems because of its sustainable and environmentally friendly advantages [5, 6]. Yahya et al. [7] experimentally investigated the solar assisted HPD and found that the average COP and SEMR were 3.7 and 0.24 kg·kWh−1, respectively. Singh et al. [8] proposed a solar assisted HPD with hot water cycle and found that compared with conventional HPD, the COP and SEMR of solar assisted HPD were improved by 68.13 % and 59.9 %, respectively. Li et al. [9] carried out an experimental study on the solar assisted HPD with a large environment temperature difference. The results showed that under the load condition, the COP of solar assisted HPD was improved by 83.3 % compared with that of conventional HPD. Dong et al., [10, 11] experimental investigated the solar assisted heat pump system by a variable frequency compressor and found that the average daily electrical efficiency of solar assisted system is 6.25 % higher than that of uncooled PV panel. Yu and Yu [11] simulated a solar assisted quasi-two-stage compression HPD and found that the proposed system could absorb the solar energy at very low temperature. The COP of solar assisted HPD was improved by 21.8 % compared with that of conventional HPD. Although the solar-assisted HPD systems achieve many performance advantages, the performance of solar assisted HPD systems could be further improved by introducing an ejector into the systems.

There is a large expansion work loss caused by the expansion device in the refrigeration/heat pump system, which could be recovered by the ejector without consuming any electric power consumption [12]. The using of ejector in the HPD system has become an appropriate method to improve the system performance. Chen et al. [13] introduced an ejector into a solar assisted heat pump water heater system to recover the expansion work and improve the heat pump performance. The experimental results indicated that the COP of ejector enhanced system was improved by 29 % compared with that of conventional system. Zhang et al. [14] presented a novel ejector enhanced heat pump system using the CO_2 as the refrigerant. The COP, exergy efficiency and irreversibility per unit heating capacity of ejector enhanced system were improved by 14.83 %, 38.14 % and 10.26 % compared with those of conventional heat pump system, respectively. Yu and Yu [15] applied an ejector and a subcooler in the HPD and found that the higher degree of supercooling of subcooler could be obtained by the ejector. Yu and Yu [26] carried out the theoretical investigation on the optimum intermediate pressure of solar-air double source HPD with an injection type compressor and an ejector. The results indicated that COP of ejector enhanced system was improved by 36.6 % compared with that of conventional heat pump system under the optimum intermediate pressure. Lu et al.[16] proposed a dual ejector enhanced heat pump cycle with three-evaporators and found that more expansion work could be recovered and better temperature match between the refrigerant and air at the evaporator could be achieved. The COP of ejector enhanced cycle was improved by 26.1 % and the exergy destruction was reduced by 28.6 % compared with those of conventional cycle. There are many theoretical researches about the solar assisted ejector enhanced HPD systems. However, to our best knowledge, there is no previous study on such a specific topic of experimental investigation. In fact, the drying characteristics and the optimal operating parameters of the HPD system will be changed after the introduction of solar energy and ejector. The comprehensive experimental investigation is necessary to develop a novel HPD system.

In the previous study [17, 18], the authors have presented a solar assisted ejector enhanced heat pump cycle in which the solar energy heats the vapor refrigeration from the condenser and it serves as the primary fluid to drive the ejector. In this study, we extend previous theoretical and experimental research by experimentally investigating the impact of different ejector configurations on the drying characteristics of a solar-assisted ejector-enhanced heat pump dryer (SE-HPD) system. This paper mainly studies the influence of the throat diameter of the nozzle, the throat diameter of the mixing chamber and the nozzle exit position on the dynamic working characteristics of the system and the ejector.

2. Experimental apparatus and test method

2.1. System description

The SE-HPD system main contains the heat pump system, the drying chamber system and the hot-water cycle system. Fig. 1 displays the schematic diagram of the heat pump system of SE-HPD. The main components of SE-HPD include an injection type compressor, a condenser, a double-pipe exchanger, a separator, an ejector, an evaporator and three electronic expansion valves (EV). The photograph of experimental facility of SE-HPD is showed in Fig. 2. The structure of the injector is shown in Fig. 3.

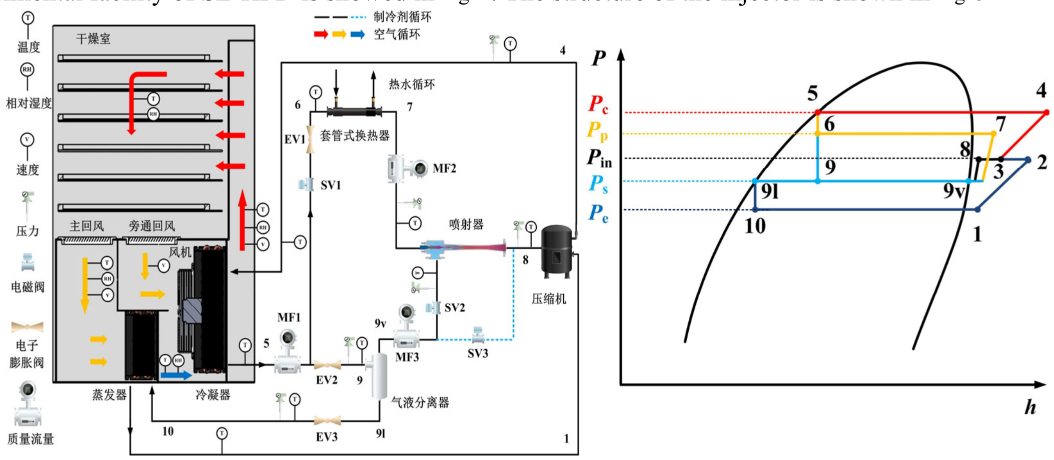

(a) Schematic diagram a of SE-HPD (b) P-h diagram of SE-HPD

Fig. 1. Schematic diagram and P-h diagram of heat pump experimental system of SE-HPD

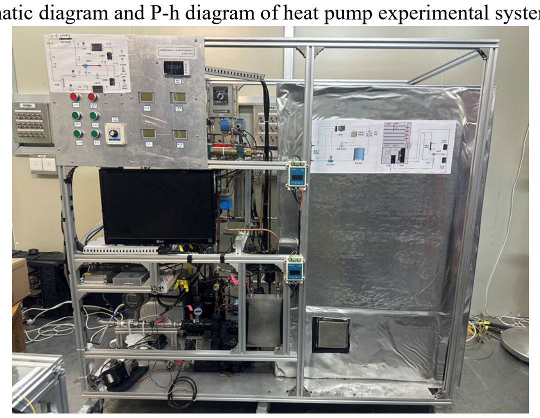

(a) Experimental facility of SE-HPD

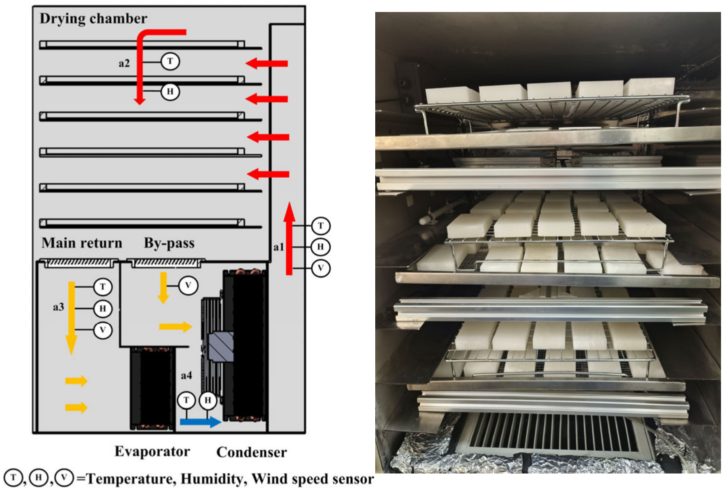

(b) Schematic diagram of the drying chamber and the drying product

Fig. 2. Photograph of experimental facility of SE-HPD

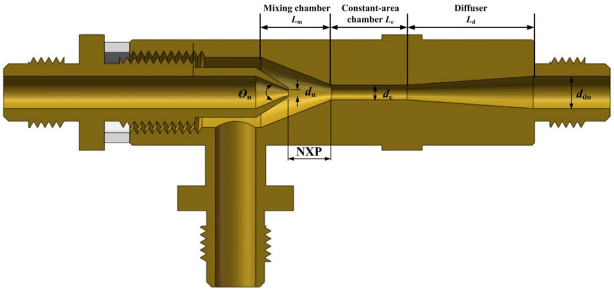

Fig. 3. Schematic diagram of an ejector

The experimental facility can operate at two different working modes: the solar energy assisted ejector enhanced heat pump drying mode (SE-HPD) and the conventional heat pump drying mode (CHPD). The experimental facility realizes the mode changing by switching the solenoid valves (SV), and the specific method for changing the working mode can be found in the Table.1. For a detailed introduction to the system and the specific parameters of its configuration, please refer to our published papers [18].

Table 1. The method for changing the working mode of the experimental facility

Mode	SV1	SV2	SV3
CHPD	OFF	OFF	ON
SE-HPD	ON	ON	OFF

2.2. Experimental instrumentation

The specifications of system components are shown in Table 2. In this study, a variable speed compressor has been applied to control the heating capacity and drying temperature. In this case, the SE0HPD can achieve the same drying temperature as the CHPD at a relatively lower compressor speed, so it has great energy saving potential. A close-loop drying chamber with a volume of 300 L has been applied. In this drying chamber, a fin tube heat exchanger fitted with a fan is utilized as a condenser. And the other fin tube heat exchanger is used as an evaporator. Three electronic expansion valves are adopted as the throttling devices. In addition, an ejector with convergent nozzle is applied to increase the refrigerant pressure. According to Fig.1, the lower pressure at the separator could be obtained at the same intermediate pressure attributed to the ejector's pressure lift ratio. As a result, the enthalpy value of the refrigerant before entering the evaporator is reduced, resulting in an increase in cooling capacity of the evaporator. The more specified data including the ejector designed parameters can be found in the previous paper [18].

Table 2. The specifications of system components

System Components	Specifications
Compressor	Hermetic rotary DC inverter compressor Cylinder volume = 14.9 cm^3, Revolution range: 1800 RPM – 7200 RPM This paper: 3000RPM Refrigerant type: R134a
Fan	Axial flow fan with brushless DC motor Revolution: 3000 RPM Air flow =1730 $m^3 \cdot h^{-1}$
Drying chamber	Type: close-loop and trays volume= 300 L
Double pipe heat interchanger	$D_{inner\ tube}$=9.52 mm, $D_{out\ tube}$ = 20 mm, length= 3.3m
Separator	Type: gravity separator
Evaporator	heat exchange area=10.2 m^2
Condenser	heat exchange area=13.7 m^2
Ejector	Type: convergent nozzle reference to paper[18]

In order to acquire the drying characteristics, a number of sensors are used in the dryer system. The detail specifications and uncertainties of sensors are shown in Table.3.

Table 3. the specifications and uncertainties of sensors

Parameter	Specifications	Uncertainties
Temperature	T-type Thermocouple	±0.5 ℃

	Range: -250 ℃~ 350 ℃	
Pressure	Pressure sensor Range: 0 ~ 4 MPa	±0.1 %
Relative humidity	Psychrometer Range: 5 % RH ~ 95 % RH	±1 % RH
Weight of drying product	Weight sensor Range: 0 ~ 10 kg	± 0.3 %
Speed of air	Thermal anemometer Range: 0 ~ 15 $m \cdot s^{-1}$	± 0.2 %
Electric power	Electrodynamometer Range: 0 ~ 99999 kWh	± 0.2 %
Mass flow rate	Coriolis mass flow meter Range: 0 ~ 200 $kg \cdot h^{-1}$	± 0.2 %

2.3. Data reduction

The electric power and the flow rate of water could be controlled by adjusting the gear pump and the AC voltage regulator through the computer program. This program is written by the Labview language. In detail, the desired simulated solar energy $Q_{\mathrm{s,\,sim}}$ could be calculated by the present parameters of collector[19, 20]:

$$Q_{\mathrm{s,sim}} = A_{\mathrm{sc}} F_{\mathrm{R}} \left[G(\alpha\tau) - U_{\mathrm{L}} \left(T_{\mathrm{sc}} - T_{\mathrm{a}} \right) \right] \tag{1}$$

where A_{sc} is the area of solar collector, T_{sc} is the temperature of solar collector, respectively, G is the solar radiation intensity, F_{R} is the collector heat removal factor, $\alpha\tau$ is the transmittance-absorptance product, U_{L} is the heat loss coefficient, T_{a} is the ambient temperature.

The actual heat exchange capacity in the double pipe heat interchanger can be acquired obtained by the follow equation. By adjusting the electrical power and the flow rate of hot water, the actual heat transfer Q_{s} could track the simulated solar energy $Q_{\mathrm{s,\,sim}}$ in time.

$$Q_{\mathrm{s}} = C_{\mathrm{p}} q_{\mathrm{w}} \rho_{\mathrm{w}} \left(T_{\mathrm{w,\,in}} - T_{\mathrm{w,\,out}} \right) \tag{2}$$

where $T_{\mathrm{w,\,in}}$ and $T_{\mathrm{w,\,out}}$ are the water temperatures at the inlet and outlet of double-pipe heat exchanger, C_{p} is the specific heat of water, ρ_{w} is the density of water, q_{w} is the flow rate of water.

The state parameters of refrigerant, air, hot water and drying product, such as the temperature, humidity, pressure, and etc have been measured to evaluate the system performance. In this study, the following drying performances parameters are studied: the moisture extraction rate (MER), the specific moisture extraction rate (SMER) and the coefficient of performance (COP).

The MER represents the drying rate at which the HPD system drying product. It equals to the ratio of the moisture taken away by the hot air to the time it costs, which is calculated by:

$$\mathrm{MER} = m_{\mathrm{w}} / t_{\mathrm{d}} \tag{3}$$

where m_{w} is the water taken away by the hot air, which can be calculated from:

$$m_{\mathrm{w}} = m_{\mathrm{pi}} - m_{\mathrm{pt}} \tag{4}$$

where m_{pi} and m_{pt} are the weight of products at the last time and present time, respectively. And t_{d} is the drying time during this period. For steady-state experiments, this t_{d} is equal to the time during entire drying process. And for dynamic experiments, this t_{d} is equal to 10 minutes in this study.

The SMER represents the energy consumption level of HPD system. And it equals to the ratio of moisture taken away by the hot air to the total electric consumption, which is calculated by:

$$\mathrm{SMER} = m_{\mathrm{w}} \Big/ \left[\left(W_{\mathrm{c}} + W_{\mathrm{f}} \right) t_{\mathrm{d}} \right] \tag{5}$$

where W_{c} and W_{f} are the electricity consumption of compressor and fan, respectively.

The moisture content (MC) represents the amount of water in product at any time, which can be given as:

$$\mathrm{MC} = \left(m_{\mathrm{pt}} - m_{\mathrm{d}} \right) \Big/ m_{\mathrm{pt}} \tag{6}$$

where m_{d} is the weight of drying product.

The COP represents the energy utilization of HPD system, which can be calculated by:

$$\mathrm{COP} = Q_{\mathrm{con}} / \left(W_{\mathrm{c}} + W_{\mathrm{f}} \right) \tag{7}$$

where Q_{con} is the heating capacity, which can be expressed as:

$$Q_{\mathrm{con}} = m_4 \left(h_4 - h_5 \right) \tag{8}$$

The ejector is an important component in SE-HPD to recover the expansion power and increase the refrigerant pressure. The entrainment ratio μ and pressure lift ratio have been chosen as the important performance indexes, which can be calculated by:

$$r_{\mathrm{pj}} = p_8 / p_{9\mathrm{v}} \tag{9}$$

$$\mu = m_{9\mathrm{v}} / m_7 \tag{10}$$

The relative uncertainty U_{y} is acquired by the follow equations [13]:

$$\mathrm{y} = f\left(x_1, x_2, \cdots\cdots, x_N \right) \tag{11}$$

$$U_{\mathrm{y}} = \sqrt{\sum_{1}^{\mathrm{n}} \left(\frac{\partial y}{\partial x_{\mathrm{i}}} \frac{u_{\mathrm{i}}}{y} \right)^2} \tag{12}$$

Based on the above equations, the relative uncertainties of the COP, MER, SMER, entrainment ratio and pressure lift ratio are 0.73%, 1.21%, 1.24%, 0.57 % and 0.28 %, respectively.

Based on Equations (1) and (2), the actual heat transfer rate in the tube-in-tube heat exchanger can be dynamically adjusted to track the simulated solar heating rate by regulating the hot water flow rate via a gear pump controller and the electric heating power via an AC voltage regulator. The specific control logic is illustrated in Fig. 4. At the start of each simulation cycle, initial values for the gear pump flow rate ($q_{\mathrm{v},0}$) and the heater voltage (U_0) are set. Combining the temperature differences $T_{\mathrm{w,in}}$-$T_{\mathrm{w,out}}$, and out at the inlet and outlet of the hot water in the tubular heat exchanger, the actual heat exchange capacity Q_{s} in the tubular heat exchanger at the initial moment can be calculated through equation (2). Compare the actual heat exchange quantity Q_{s} with the simulated solar heating quantity $Q_{\mathrm{s,sim}}$ and sim calculated in Equation (1).

If the discrepancy between Q_{s} and $Q_{\mathrm{s,sim}}$ is less than 5%, the current heat exchanger performance is deemed satisfactory. In this case, no adjustments are made, and the current values $q_{\mathrm{v},0}$ and U_0 are directly assigned to the next cycle as $q_{\mathrm{v},1}$ and U_1。 If the error exceeds 5%, a new flow rate for the next cycle is calculated as $q_{\mathrm{v},1} = q_{\mathrm{v},0}\sqrt{Q_{\mathrm{s,sim}}/Q_{\mathrm{s}}}$. The value of $q_{\mathrm{v},1}$ is then evaluated:

If $q_{\mathrm{v},1}$ is greater than the maximum set flow rate ($q_{\mathrm{v,max}}$=4 L·min^{-1}), the heater power must be increased by setting the next cycle's voltage to U_1= 1.5U_0.

If $q_{\mathrm{v},1}$is between the minimum ($q_{\mathrm{v,min}}$=2 L·min^{-1}) and maximum set flow rates, the heater power remains unchanged: U_1= U_0.

If $q_{\mathrm{v},1}$ is less than the minimum set flow rate, the heater power is decreased: U_1=0.7U_0.

At the end of each cycle, the initial values $q_{\mathrm{v},0}$ and U_0 are updated, and the next cycle begins. In this experiment, based on the operational ranges and characteristics of the components, each control cycle has a duration of 20 seconds.

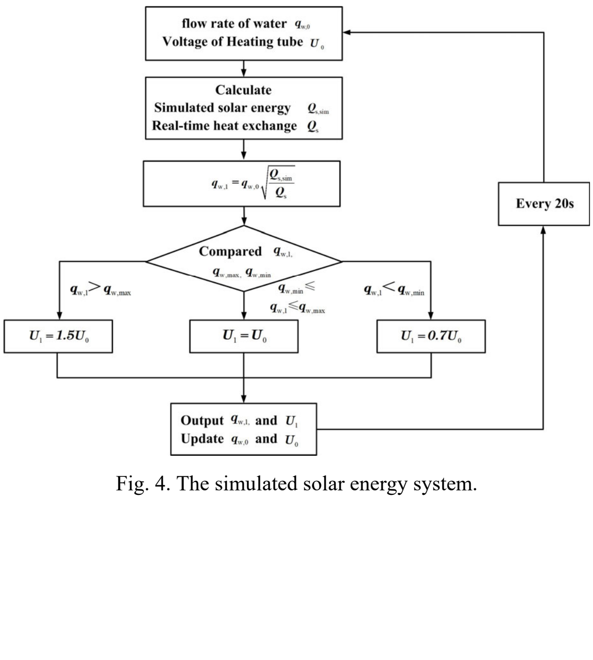

Fig. 4. The simulated solar energy system.

2.4. Drying product of experiment

The developed experimental facility is designed for drying any wet products and the experiment is carried out to study the dynamic and steady drying characteristic of SE-HPD and CHPD. Considering that a large number of experiments need to consume a lot of experimental products, this will cause a serious waste of resources. Therefore, this paper uses the sponges as the drying product of experiment. The sponge not only has a high moisture content (the moisture content of the sponge can reach to 99.9 % after absorbing water), but also can be reused by absorbing the water after the drying experiment.

3. Results and discussion

The structural parameters of the ejector also have a significant impact on the state parameters and drying performance of the system. This section mainly studies the influence of the throat diameter of the nozzle, the throat diameter of the mixing chamber and the nozzle exit position on the dynamic working characteristics of the system and the ejector. The nozzle used in this experiment is a gradually shrinking adjustable nozzle. The diameter of its throat can be adjusted by the movement distance of the adjustable needle. The equivalent diameter calculation formula of the nozzle throat could be found in the reference [18]. In this paper, the equivalent diameter of the nozzle throat is represented by the axial movement distance x of the adjustable needle, and the result is shown in Fig. 5.

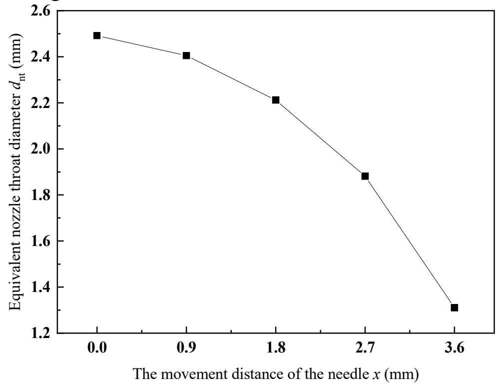

Fig. 5. The relationship between the equivalent diameter of the nozzle throat and the axial movement distance of the adjustable needle

3.1. The effect of the nozzle throat diameter

Fig. 6 illustrates the impact of nozzle throat diameter variation (1.31-2.49 mm corresponding to adjustable needle displacement of 0-3.6 mm) on the dynamic drying performance of the Solar-assisted Ejector-enhanced Heat Pump Dryer (SE-HPD). The results demonstrate a clear optimal value for the nozzle throat diameter regarding system performance. As the needle advances from 0 mm to 1.8 mm (throat diameter decreasing to 2.21 mm), both the moisture extraction rate (MER) and specific moisture extraction rate (SMER) increase significantly, reaching peak values of 1.65 kg·h^{-1} and 1.76 kg·(kWh)$^{-1}$, respectively. This represents a performance improvement over the initial values at 0 mm displacement (MER: 1.45 kg·h^{-1}, SMER: 1.50 kg·(kWh)$^{-1}$). However, further advancement of the needle beyond 1.8 mm up to 3.6 mm leads to a notable decline in drying performance, with MER and SMER decreasing to 1.40 kg·h^{-1} and 1.67 kg·(kWh)$^{-1}$, respectively. This non-monotonic relationship confirms the existence of an optimal nozzle throat diameter (2.21 mm in this configuration) for maximizing the SE-HPD system's drying efficiency, beyond which performance deteriorates due to changes in ejector entrainment dynamics and refrigerant flow characteristics.

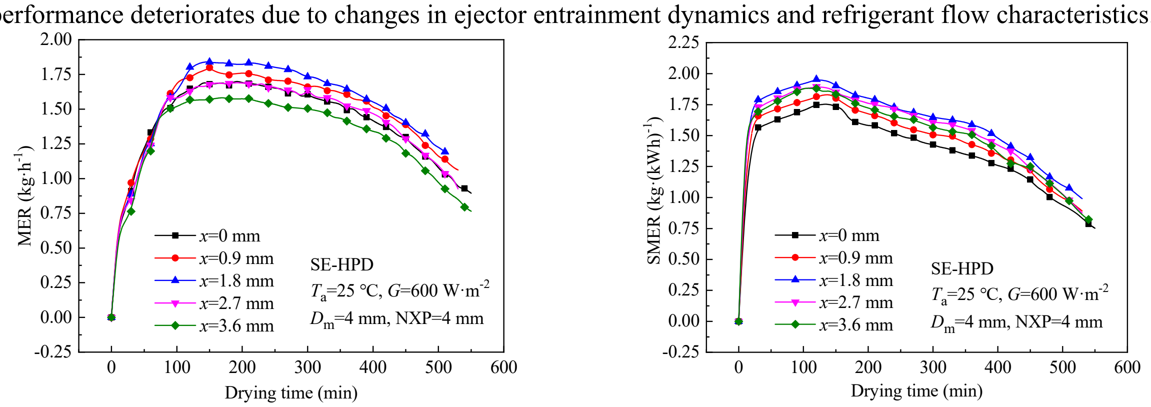

(a) MER (b) SMER

Fig. 6. Effect of the nozzle throat diameter on the dynamic drying performance of the system.

Fig. 7 illustrates the significant impact of nozzle throat diameter variation on the dynamic heating performance of the SE-HPD system. The data reveals a clear performance threshold: as the adjustable needle advances from 0 mm to 1.8 mm, the condenser's heating capacity remains stable at approximately 3800 W. However, further advancement beyond this point: corresponding to a continued reduction in throat diameter, triggers a progressive decline in heating capacity, which falls to around 3100 W.

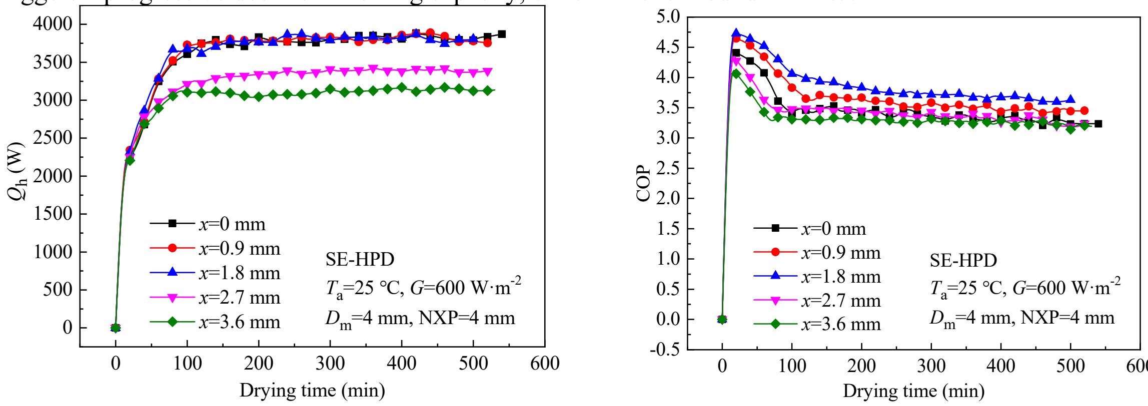

(a) heating capacity (b) COP

Fig. 7. Effect of nozzle throat diameter on the dynamic heating performance of heat pump systems

Fig. 7 reveals a non-linear relationship between the nozzle throat diameter and the system's heating performance coefficient (COP). When the adjustable needle advances to 1.8 mm (corresponding to a nozzle throat diameter of 2.21 mm), the COP increases significantly from 3.28 to 3.62. This improvement stems from a dual mechanism: the reduced nozzle diameter increases flow resistance in the solar branch, redirecting more refrigerant to the evaporator branch, while the ejector's reduced pressure-lift capacity synergistically increases evaporator pressure from 675.4 kPa to 718.5 kPa, as shown in Fig. 9. The resulting increase in evaporator cooling capacity combined with decreased compressor power consumption enhances both COP and moisture extraction rates (MER and SMER), consistent with the trends in Fig. 6. However, further needle advancement to 3.6 mm causes a sharp COP decline to 3.21. The excessively small nozzle throat diameter severely degrades ejector performance, reducing primary and secondary fluid flows, compressor gas intake, and overall refrigerant flow rate. This "solar circuit blockage" phenomenon shifts system operation toward conventional heat pump drying (CHPD) mode, evident in the condenser heating capacity reduction and evaporator pressure drop to 598.7 kPa, ultimately decreasing MER and SMER as confirmed in Fig. 6. These results demonstrate the critical optimal range for nozzle throat diameter in maximizing SE-HPD system efficiency.

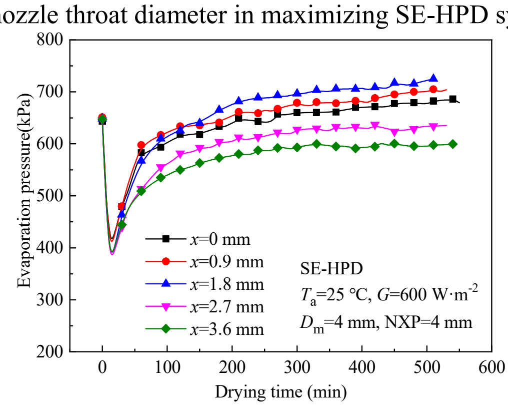

Fig. 8. The variation of evaporation pressure with drying time under different nozzle throat diameters

Fig. 9 illustrates the significant impact of nozzle throat diameter variation on the dynamic working characteristics of the ejector. The data demonstrates a clear optimum for the ejector's entrainment ratio. When the adjustable needle advances to 1.8 mm (reducing the nozzle throat diameter to 2.21 mm), the entrainment ratio increases substantially from 0.47 to 0.68. This enhancement is attributed to a dual mechanism: the reduced primary fluid flow rate, combined with the decreased spatial occupation by the primary fluid in the mixing chamber, creates favourable conditions for enhanced secondary fluid entrainment.

Concurrently, the ejector's pressure-boosting capacity exhibits a consistent decline with decreasing nozzle diameter. As shown in Fig. 9b, the maximum pressure lifting ratio (r_{pj}) decreases from 1.12 to 1.06, while the minimum stable value drops from 1.04 to 1.02. This reduction in pressure lift capacity is directly linked to the diminished pressure differential between the primary and secondary fluids caused by the smaller nozzle throat diameter. The study thus identifies a critical operational window where nozzle geometry optimization is essential for maintaining efficient ejector performance.

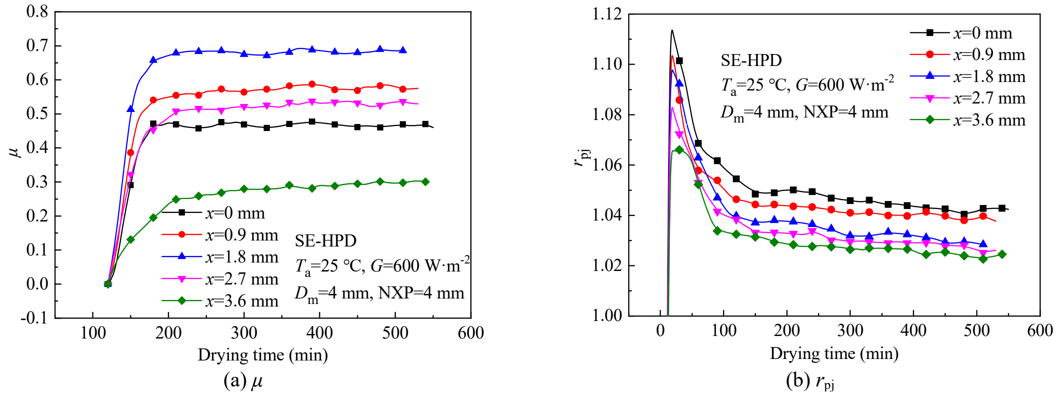

Fig. 9. The influence of the nozzle throat diameter on the dynamic working performance of the ejector

3.2. The influence of the throat diameter of the mixing chamber

The throat diameter of the mixing chamber is the outlet of the contraction section of the mixing chamber or the diameter of the mixing section with the same cross-sectional area of the mixing chamber. In this experiment, the throat diameter of the mixing chamber ranges from 3 mm to 6 mm. Fig. 10 shows the influence law of the throat diameter of the mixing chamber on the dynamic drying performance of SE-HPD. It can be seen from the figure that when the throat diameter of the mixing chamber increases from 3 mm to 5 mm, the average moisture extraction rate of SE-HPD increases from 1.37 kg·h^{-1} to 1.60 kg·h^{-1}. This is because as the diameter of the throat of the mixing chamber increases, the mixing area of the primary and secondary fluids in the mixing chamber increases, which enhances the ejection capacity of the ejector, increases the make-up air volume of the compressor, and thereby raises the heating capacity of the condenser. However, when the throat diameter of the mixing chamber continued to increase to 6 mm, the average moisture extraction rate MER of SE-HPD slightly decreased to 1.58 kg·h^{-1}. The reason for the slight decrease in the drying rate is that the diameter of the throat of the mixing chamber is too large. The diameter of the cross-section of the mixed fluid formed by the expansion of the primary fluid and the secondary fluid is smaller than that of the throat of the mixing chamber. At this time, the existence of the cavity in the mixing chamber causes the generation of vortices in the mixing chamber, which will greatly reduce the ejection performance of the ejector. Therefore, when the throat diameter of the mixing chamber increases to 6 mm, the ejection ratio of the ejector decreases, the make-up air volume of the compressor reduces, which leads to a decrease in the heating capacity of the condenser and a decrease in the moisture extraction rate MER.

The experimental results in Fig. 10 also indicate that with the increase of the throat diameter of the mixing chamber, the SMER of SE-HPD keeps increasing, from 1.35 kg·(kWh)$^{-1}$ to 1.63 kg·(kWh)$^{-1}$. The reason for the continuous increase is that as the diameter of the throat of the mixing chamber increases, the degree of compression of the secondary fluid by the contraction section of the mixing chamber decreases. Therefore, the pressure of the secondary fluid in the mixing chamber rises, and the corresponding evaporation pressure of the evaporator gradually increases as well. The pressure ratio of the compressor decreases, thereby leading to a reduction in the power consumption of the compressor.

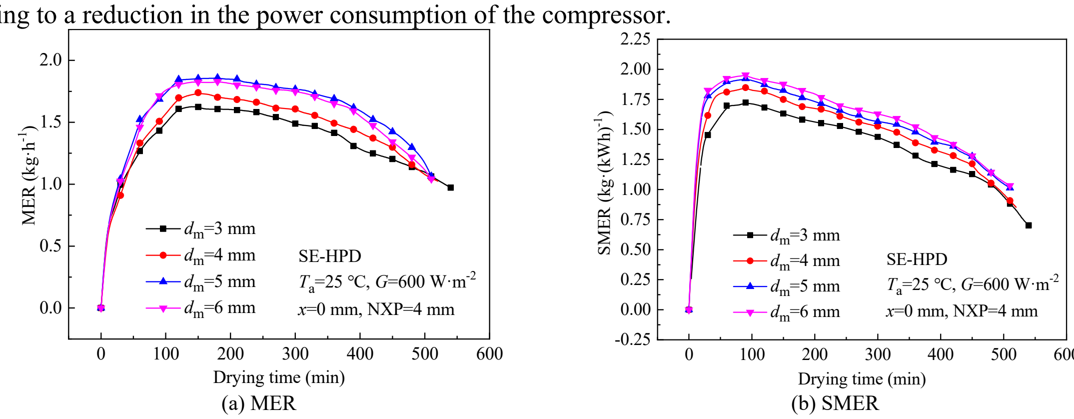

Fig. 10. The influence of the throat diameter of the mixing chamber on the dynamic drying performance of the system

Fig. 11 shows the influence law of the throat diameter of the mixing chamber on the dynamic working performance of the ejector. It can be seen from the figure that when the diameter of the throat of the mixing chamber increases from 3 mm to 5 mm, the ejection ratio of the ejector rises from 0.38 to 0.57. The reason for the increase in the ejection ratio is that when the diameter of the throat of the mixing chamber increases, the mixing area of the primary fluid and the secondary fluid in the mixing chamber increases, that is, the mixing chamber can accommodate more secondary fluid, which improves the ejection capacity of the ejector.

However, when the throat diameter of the mixing chamber is further increased to 6 mm, the ejection ratio of the ejector decreases to 0.50. The reason for the decrease in the ejection ratio is that the diameter of the throat of the mixing chamber is too large. When the diameter of the cross-section of the mixed fluid formed by the expansion of the primary fluid and the secondary fluid is smaller than the diameter of the throat of the mixing chamber, a large cavity will be generated in the mixing chamber. Vortices will be produced in the cavity and the ejection performance of the ejector will be greatly reduced.

The experimental results in Fig. 11b also show that as the diameter of the throat of the mixing chamber increases, the pressure rise ratio of the ejector gradually decreases at any drying time. Specific analysis: When the throat diameter of the mixing chamber increases from 3 mm to 5 mm, the maximum pressure rise ratio of the ejector decreases from 1.15 to 1.07, and the minimum value under stable operating conditions decreases from 1.06 to 1.03. The reason for the decrease in the pressure increase ratio of the ejector is that the pressure of the secondary fluid increases with the increase of the throat diameter of the mixing chamber, that is, the pressure difference between the primary fluid and the secondary fluid decreases, and thus the pressure increase capacity of the ejector decreases.

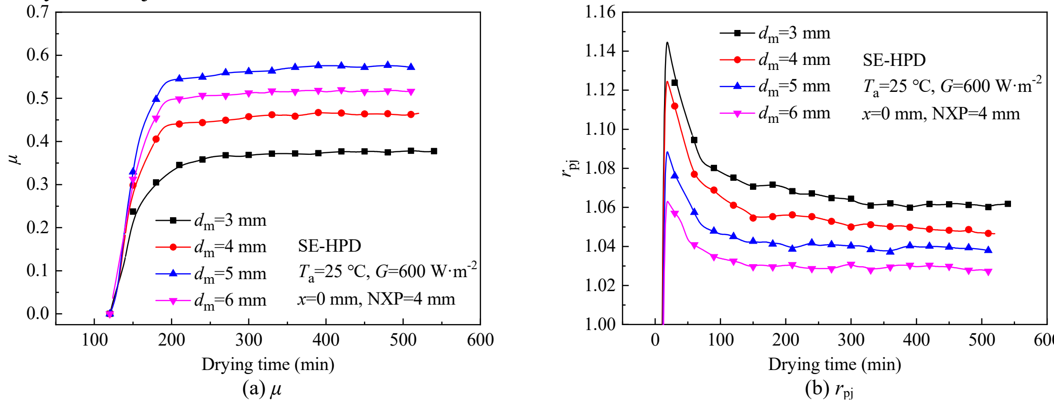

Fig. 11. The influence of the throat diameter of the mixing chamber on the dynamic working performance of the ejector

3.3. The matching relationship between the throat diameter of the nozzle and that of the mixing chamber

Fig. 12 shows the influence of the nozzle throat diameter on the ejection ratio of the ejector under different throat diameters of the mixing chamber. This study establishes that optimal performance of both the ejector and the overall heat pump drying system is achieved through a precise geometric match between the nozzle and the mixing chamber, rather than through independent optimization of their throat diameters. Experimental results reveal a direct proportional relationship: as the mixing chamber throat diameter increases from 3 mm to 5 mm, the corresponding optimal nozzle throat diameter shifts from 1.88 mm to 2.40 mm to maintain high entrainment ratios (0.68, 0.65, and 0.66, respectively). This critical interdependence arises from internal flow dynamics; a mismatched geometry—such as an overly large nozzle in a small chamber that blocks secondary flow, or an undersized nozzle in a large chamber that reduces shear and mixing efficiency—severely compromises ejector performance.

Consequently, the ejector's efficiency is best characterized by a key dimensionless parameter, the Area Ratio (AR), defined as the ratio of the mixing chamber throat area to the nozzle throat area. The findings confirm that for a given set of conditions, an optimal AR exists to maximize system performance. This concept of an optimal AR is of great significance for guiding the design of high-efficiency ejectors. However, a comprehensive exploration of the optimal AR across a wide range of conditions is limited by the experimental method, which is resource-intensive and cannot visualize internal flow mechanisms. Therefore, future work will employ CFD numerical simulation to efficiently map the influence of AR, visualize the internal fluid mixing processes, and provide a more robust foundation for determining the optimal geometric matching under various operating conditions, thereby advancing ejector design for thermal systems.

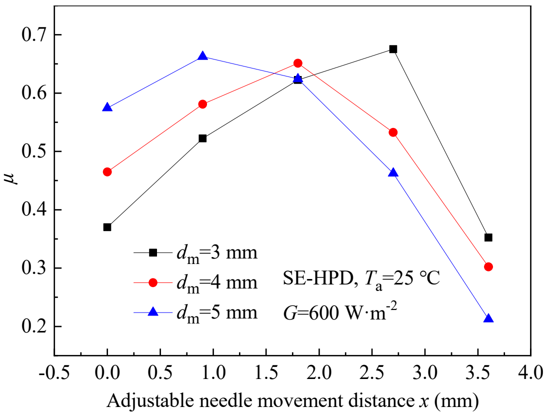

Fig. 12. The influence of the nozzle throat diameter and the mixing chamber throat diameter on the entrainment ratio

4. Conclusions

This comprehensive experimental investigation conclusively demonstrates that the dynamic performance of the Solar-assisted Ejector-enhanced Heat Pump Dryer (SE-HPD) is profoundly governed by the intricate interplay of key ejector structural parameters, with the identification of an optimal nozzle throat diameter of 2.21 mm yielding a peak system performance characterized by a moisture extraction rate (MER) of 1.65 kg·h⁻¹, a specific moisture extraction rate (SMER) of 1.76 kg·(kWh)⁻¹, and a heating coefficient of performance (COP) of 3.62. A critically important finding is the synergistic matching relationship between the nozzle and mixing chamber throat diameters, where a larger mixing chamber necessitates a correspondingly larger optimal nozzle diameter, an interdependence best characterized by a specific critical area ratio for maximum ejector entrainment ratio and system efficiency, as graphically evidenced by the experimental data. Furthermore, the nozzle exit position (NXP) is established as a crucial factor, with an optimal value of 5 mm achieving the highest entrainment ratio of 0.52, while deviations cause significant performance loss due to flow impingement. The study also reveals performance boundaries, wherein exceeding a mixing chamber throat diameter of 5 mm induces vortex effects, degrading entrainment by 12.3%. These findings provide essential experimental insights and quantitative design guidelines for dynamically optimizing ejector configuration, directly enabling the development of more efficient, adaptive, and high-performance heat pump drying systems by strategically balancing the ejector's geometry to enhance entrainment, compressor suction, and overall thermal efficiency. Ultimately, this work not only clarifies the fundamental impact of ejector design on system dynamics but also paves the way for future research employing CFD simulations to further explore the optimal AR across wider conditions and elucidate the underlying fluid mixing mechanisms.

Acknowledgements

The authors acknowledge deeply the support from the National Natural Science Foundation of China (Grant No. 52176019). References

[1] N. Colak, A. Hepbasli, A review of heat pump drying: Part 1 – Systems, models and studies, Energy Conversion and Management, 50(9) (2009) 2180-2186.
[2] N. Colak, A. Hepbasli, A review of heat-pump drying (HPD): Part 2 – Applications and performance assessments, Energy Conversion and Management, 50(9) (2009) 2187-2199.
[3] R. Daghigh, M. Ruslan, M. Sulaiman, et al., Review of solar assisted heat pump drying systems for agricultural and marine products, Renewable and Sustainable Energy Reviews, 14(9) (2010) 2564-2579.
[4] I.D. Boateng, A review of solar and solar-assisted drying of fresh produce: state of the art, drying kinetics, and product qualities, Journal of the Science of Food and Agriculture, (2023).
[5] D. Kohli, M. Sharma, P.S. Champawat, et al., Heat Pump drying of Food Product: A Review, Octa Journal of Biosciences, 10(2) (2022) 124-133.
[6] F. Salehi, Recent Applications of Heat Pump Dryer for Drying of Fruit Crops: A Review, International Journal of Fruit Science, 21(1) (2021) 546-555.
[7] M. Yahya, H. Fahmi, A. Fudholi, et al., Performance and economic analyses on solar-assisted heat pump fluidised bed dryer integrated with biomass furnace for rice drying, Solar Energy, 174 (2018) 1058-1067.
[8] A. Singh, J. Sarkar, R. Rekha Sahoo, Experimentation on solar-assisted heat pump dryer: Thermodynamic, economic and exergoeconomic assessments, Solar Energy, 208 (2020) 150-159.
[9] J. Li, Y. Zhang, M. Li, et al., Study on heating performance of solar-assisted heat pump drying system under large temperature difference, Solar Energy, 229 (2021) 148-161.
[10] D. Zhang, S. Xinyue, L. Pengfei, et al., Experiment study on startup characteristics and operation performance of PV/T solar assisted heat pump water heater system driven by direct current variable frequency compressor, Solar Energy, 263 (2023).
[11] J. Yu, J. Yu, Simulation study of a heat pump drying system using a solar assisted flash tank vapor injection cycle, Solar Energy, 251 (2023) 223-239.

[12] Z. Zhang, X. Feng, D. Tian, et al., Progress in ejector-expansion vapor compression refrigeration and heat pump systems, Energy Conversion and Management, 207 (2020).
[13] J. Chen, G. Zhang, D. Wang, Experimental investigation on the dynamic characteristic of the direct expansion solar assisted ejector-compression heat pump cycle for water heater, Applied Thermal Engineering, 195 (2021).
[14] Y. Zhang, X. Wei, X. Qin, Experimental study on energy, exergy, and exergoeconomic analyses of a novel compression/ejector transcritical CO2 heat pump system with dual heat sources, Energy Conversion and Management, 271 (2022).
[15] M. Yu, J. Yu, Theoretical study of a modified ejector enhanced vapor injection heat pump cycle with hybrid solar-air source for dryer application, Solar Energy, 248 (2022) 171-182.
[16] X. Yu, W. Wu, J. Wang, et al., Experimental study on effect of drying air supply temperature on performance of a quasi-two-stage closed loop heat pump drying system for lentinus edodes, Renewable Energy, 201 (2022) 1038-1049.
[17] X. Lv, M. Yu, J. Yu, Performance analysis of an ejector-boosted solar-assisted flash tank vapor injection cycle for ASHP applications, Solar Energy, 224 (2021) 607-616.
[18] M. Yu, L. Zou, J. Yu, Experimental investigation on the drying characteristics in a solar assisted ejector enhanced heat pump dryer system, Solar Energy, 267 (2024).
[19] W. Pridasawas, P. Lundqvist, An exergy analysis of a solar-driven ejector refrigeration system, Solar Energy, 76(4) (2004) 369-379.
[20] M. Oliveira, J.C. Charamba Dutra, The impact of the V-corrugation on the thermal efficiency of a solar collector, Solar Energy, 255 (2023) 460-473.